Nuclear Science and Techniques (2026) 37:123
https://doi.org/10.1007/s41365-026-01938-x

Probing jet-medium interactions via jet substructure observables in relativistic heavy-ion collisions

Xiang-Pan Duan[1,2,3] · **Tan Luo**[4] · **Guo-Liang Ma**[1,2]

Received: 30 June 2025 / Revised: 10 August 2025 / Accepted: 8 September 2025 / Published online: 15 April 2026

Abstract
We present a comprehensive study of jet substructure observables in pp and PbPb collisions at $\sqrt{s_{\mathrm{NN}}} = 5.02$ TeV using a multi-phase transport model. To suppress background contamination, the constituent subtraction method was employed for both PbPb and smeared pp events. The jet splitting momentum fraction (z_{g}) and the ratio of the groomed jet mass to the ungroomed jet transverse momentum ($M_{\mathrm{g}}/p_{\mathrm{T,jet}}$) were reconstructed using the Soft Drop algorithm with two grooming parameter settings. With $z_{\mathrm{cut}} = 0.1$ and $\beta = 0.0$, a slight modification in the z_{g} distribution is observed in central PbPb collisions, whereas a pronounced enhancement in the high $M_{\mathrm{g}}/p_{\mathrm{T,jet}}$ region is found, particularly at low $p_{\mathrm{T,jet}}$ and in more central events. A detailed analysis of the dynamical evolution stages revealed that this enhancement primarily originates from jet–medium interactions, whereas the contributions from hadronization and hadronic rescatterings are largely mitigated by the grooming procedure. In contrast, under a stronger grooming condition ($z_{\mathrm{cut}} = 0.5$, $\beta = 1.5$), no significant changes in $M_{\mathrm{g}}/p_{\mathrm{T,jet}}$ are observed, indicating that the medium-induced modifications are predominantly associated with large-angle scattering within the AMPT framework.

Keywords Heavy-ion collisions · Jet quenching · Quark-gluon plasma · Transport model

1 Introduction

Relativistic heavy-ion collisions at the Relativistic Heavy Ion Collider (RHIC) [1–8] and the Large Hadron Collider (LHC) [9–14] create an extremely hot and dense nuclear matter referred to as the quark-gluon plasma (QGP) [15, 16]. In the early stages of the collisions, hard scatterings governed by quantum chromodynamics (QCD) produce high-energy partons with large virtualities. These partons subsequently undergo parton showering and evolve into collimated sprays of hadrons, referred to as jets [17, 18]. As these energetic partons traverse the QGP medium, they

This work was supported by the National Natural Science Foundation of China (Nos. 12147101, 12547102, and 12325507), the National Key Research and Development Program of China (No. 2022YFA1604900), the Guangdong Major Project of Basic and Applied Basic Research (No. 2020B0301030008 (X.D. and G.M.)), the China Scholarship Council (No. 202306100165), the European Research Council project ERC-2018-ADG-835105 YoctoLHC, the Maria de Maeztu grant CEX2023-001318-M and the project PID2023-152762NB-I00 both funded by MCIN/AEI/10.13039/-501100011033, the Xunta de Galicia (CIGUS Network of Research Centres), and the European Union (X.D.).

✉ Xiang-Pan Duan
xpduan20@fudan.edu.cn

✉ Tan Luo
luotan@hnu.edu.cn

✉ Guo-Liang Ma
glma@fudan.edu.cn

[1] Key Laboratory of Nuclear Physics and Ion-beam Application (MOE), Institute of Modern Physics, Fudan University, Shanghai 200433, China

[2] Shanghai Research Center for Theoretical Nuclear Physics, NSFC and Fudan University, Shanghai 200438, China

[3] Instituto Galego de Física de Altas Enerxías IGFAE, Universidade de Santiago de Compostela, E-15782 Galicia, Spain

[4] School of Physics and Electronics, Hunan University, Changsha 410082, China

undergo multiple interactions, including medium-induced gluon radiation and elastic scattering, resulting in energy loss and transverse momentum broadening. This phenomenon is known as jet quenching [19–27], which leads to observable modifications in jet properties. Currently, jet quenching has become a widely used probe for accessing the transport properties of QGP. Measurements of jet observables, such as nuclear modification factor [28–35], di-/γ-/Z-jet momentum imbalance [36–40], and jet transport coefficient [41, 42], provide valuable insight into parton energy loss mechanisms and the characteristics of QGP medium.

In recent years, jet substructure observables have emerged as powerful tools for probing the jet–medium interactions. By examining the substructure of reconstructed jets, such as jet splitting momentum fraction (z_g) [43–47], jet splitting radius (r_g) [44, 45], and groomed jet mass (M_g) [48–50], these observables provide direct access to the mechanisms by which QGP modifies parton shower evolution. Jet grooming algorithms have been developed to remove the soft components, thereby isolating the hard components associated with the initial parton shower and finding the corresponding pair of subjets from the reconstructed jets.

A key motivation for studying groomed jet substructure lies in its sensitivity to jet–medium interactions in relativistic heavy-ion collisions. Both experimental measurements and theoretical predictions have reported diverse trends across various kinematic regimes and grooming conditions. For instance, as measured by the CMS experiment [43], the z_g distribution in central PbPb collisions at high jet transverse momentum ($p_{T,jet} > 140$ GeV) exhibits a slight shift toward asymmetric splittings compared to peripheral PbPb and pp collisions. This observation is consistent with the predictions from several theoretical models, including JEWEL [51] and SCET [52]. At lower jet transverse momentum ($60 < p_{T,jet} < 100$ GeV), the ALICE experiment [45] reports no significant modification of the z_g distribution under strong grooming conditions, in line with the results from JETSCAPE [53]. Interestingly, the higher twist formalism [54] predicts the strongest z_g modification at intermediate jet energies, with weaker effects at both lower and higher energies.

The groomed jet mass has emerged as a sensitive observable for probing jet–medium interactions in relativistic heavy-ion collisions. Measurements by CMS experiment [48] show a significant enhancement in high $M_g/p_{T,jet}$ region in central PbPb collisions, consistent with predictions from JEWEL [55] and LBT [56] models that incorporate medium response effects. In contrast, the ALICE experiment reports a narrowing of the groomed jet mass distribution in the most central PbPb collisions compared to pp collisions [50], in agreement with the results from the Hybrid model [57] without elastic Molière scattering [58]. Notably, when elastic Molière scattering is included in the Hybrid model, a hint of enhancement in the high M_g region is observed, which is attributed to the increased contributions from large-angle jet constituents. Similar behaviors are also observed in ungroomed jet mass distributions [50], which are influenced by both perturbative and non-perturbative QCD [59]. Our previous study [59] demonstrated that the ungroomed jet mass is strongly affected by hadronization and hadronic rescatterings, which can be substantially suppressed through the application of grooming techniques. A systematic investigation of jet substructure observables across different dynamic stages of jet evolution thus provides a valuable approach for understanding jet–medium interactions in relativistic heavy-ion collisions.

The measurements of z_g and $M_g/p_{T,jet}$ serve as probes of jet quenching effects and provide valuable insights into the properties of QGP. However, the interpretation of these observables is complicated by the interplay between jet energy loss, medium response, and background fluctuations. In this context, theoretical modeling is crucial for disentangling these competing effects. In this study, we employed a multi-phase transport (AMPT) model to investigate the modification of jet substructures in pp and PbPb collisions at $\sqrt{s_{NN}} = 5.02$ TeV. We focus on the z_g and $M_g/p_{T,jet}$ observables and compare our results with the experimental measurements from CMS [43, 48]. We further explored the dependence of these observables on the jet transverse momentum, event centrality, and different dynamic stages of jet evolution, both with and without partonic interactions, to gain a deeper insight into the jet substructure modifications.

The remainder of this paper is organized as follows. In Sect. 2, we describe the AMPT framework, the jet reconstruction procedure, and the implementation of Soft Drop grooming. Section 3.1 presents the results for z_g. In Sect. 3.2, we report the results of $M_g/p_{T,jet}$ and analyze the dependence on the dynamical evolution stages. Finally, a summary is given in Sect. 4.

2 Methodology

2.1 The AMPT model

The AMPT model with the string melting mechanism, which is widely used in relativistic heavy-ion collision studies, comprises four main stages [60, 61]: initial conditions, parton cascade, hadronization, and hadronic rescatterings.

(1) *Initial conditions.* The heavy-ion jet interaction generator (HIJING) model [62, 63] provides the initial conditions for pp, pA, and AA collisions. Within the string melting mechanism, the primary interactions comprise two components: a soft contribution modeled by Lund string fragmentation [64–66] and a hard contribution from minijet

production. The differential cross section for minijet production is computed using the perturbative QCD factorization as follows:

$$\frac{d\sigma_{\text{jet}}^{cd}}{dp_{\text{T}}^2 dy_1 dy_2} = K \sum_{a,b} x_1 f_a(x_1, Q^2) x_2 f_b(x_2, Q^2) \frac{d\hat{\sigma}^{ab\to cd}}{d\hat{t}}, \quad (1)$$

where p_{T} is the transverse momentum of the produced minijet parton, y_1 and y_2 denote the rapidities of the final produced partons c and d, the factor K accounts for higher-order corrections beyond leading order (LO), and x_1, x_2 are the momentum fractions of the incoming partons a and b. The parton distribution functions (PDFs) $f_a(x_1, Q^2)$ and $f_b(x_2, Q^2)$ follow the Duke–Owens parametrization [67] with the factorization scale Q^2. The parton cross section $d\hat{\sigma}^{ab\to cd}/d\hat{t}$ is determined by the LO matrix element squared $|\mathcal{M}_{ab\to cd}|^2$, expressed in terms of the Mandelstam variables $\hat{s}$, $\hat{t}$, and $\hat{u}$. A jet-triggering technique is employed in HIJING to generate dijet events, incorporating hard scattering processes such as $qq' \to qq'$, $qq \to qq$, $q\bar{q} \to q'\bar{q}'$, $q\bar{q} \to q\bar{q}$, $gq \to gq$, $q\bar{q} \to gg$, $gg \to q\bar{q}$, and $gg \to gg$ [64, 68].

(2) *Parton cascade.* The Zhang's parton cascade (ZPC) model describes partonic interactions via two-body elastic scatterings [69]. The parton cross section for gluon–gluon scattering is evaluated at LO pQCD as

$$\sigma_{gg} \approx \frac{9\pi\alpha_s^2}{2\mu^2}, \quad (2)$$

where α_s is the strong coupling constant and μ is the Debye screening mass. Varying μ allows for the adjustment of the parton cross section in simulations.

(3) *Hadronization.* Hadronization is modeled using the quark coalescence mechanism [60], which recombines the nearest two or three partons into mesons and baryons, without considering their relative momenta. Three momentum conservations are satisfied in the coalescence process, and the hadron species are determined by the flavor and invariant mass of the coalescing partons.

(4) *Hadronic rescatterings.* The relativistic transport (ART) model [70] simulates resonance decays and hadronic reactions, including both elastic and inelastic scatterings for baryon–baryon, baryon–meson, and meson–meson interactions.

In this study, the AMPT model with the string melting mechanism was used to simulate pp and PbPb collisions at $\sqrt{s_{\text{NN}}} = 5.02$ TeV. The parton cross section was set to 3 mb, in line with previous studies that have successfully described the collective flow observed in relativistic heavy-ion collisions [71–75]. The AMPT model incorporating jet–medium interactions has been widely utilized in the investigation of various jet observables, including dijet asymmetry [37], γ-jet imbalance [76], jet fragmentation functions [77–80], jet shape [81], jet anisotropies [82], jet transport coefficients [83], the redistribution of lost energy [84–87], and jet mass [59]. For comparison, a parton cross section of 0 mb was also employed to provide a baseline scenario without jet-medium interactions.

2.2 Jet reconstruction

To measure the jet substructure observables, the jets were first reconstructed using the anti-k_t algorithm [88] with a radius parameter $R = 0.4$, as implemented in the FastJet package [89]. In this analysis, jets are required to have pseudorapidity $|\eta_{\text{jet}}| < 1.3$. To facilitate a direct comparison with the CMS measurements [43, 48], the masses of the final-state particles were adjusted such that neutral hadrons were treated as massless, whereas charged hadrons were assigned the charged pion mass, in accordance with the experimental setup used by CMS. This treatment has a non-negligible effect on the groomed jet mass distribution and is essential for a consistent comparison between the simulation and data.

In PbPb collisions, the constituent subtraction method [90] is employed to estimate the background, which is characterized by the background density ρ and background mass density ρ_{m} [89, 91]. The estimation is based on clustering particles using the k_t algorithm [92] with $R = 0.4$. Massless ghost particles with an area of 0.005 were added to the y-ϕ plane for the event. To reduce contamination from hard jet fragments, the two k_t clusters with the highest transverse momentum are excluded. Constituent subtraction is performed on a particle-by-particle basis, enabling the correction of both the jet four-momentum and its substructure. This method was applied to PbPb events generated with the AMPT model using a jet-triggering technique. To reduce the possible artifacts introduced by background subtraction in PbPb events, a smearing procedure similar to that used in the CMS experiment was adopted. Specifically, the background from PbPb collisions (without a jet trigger) is embedded into pp collisions with a jet trigger to produce the so-called smeared pp events. The constituent subtraction procedure in PbPb collisions was applied to smeared pp events to maintain consistency.

2.3 Soft drop

In addition, jet grooming is performed using the Soft Drop (SD) algorithm [93], which removes the soft components and isolates the hard components of the jet, thereby enhancing the sensitivity to medium-induced modifications. The procedure reclusters jet constituents using the Cambridge–Aachen (C/A) algorithm [94] to form a pairwise clustering tree, followed by recursive declustering. At each declustering step, the jet is separated into two subjets by reversing the last C/A clustering stage. The subjets are required to satisfy the Soft Drop condition:

$$\frac{\min(p_{\mathrm{T},1}, p_{\mathrm{T},2})}{p_{\mathrm{T},1} + p_{\mathrm{T},2}} > z_{\mathrm{cut}} \left(\frac{\Delta R_{12}}{R} \right)^{\beta}, \tag{3}$$

where $p_{\mathrm{T},1}$ and $p_{\mathrm{T},2}$ are the transverse momenta of the subjets, $\Delta R_{12} = \sqrt{(y_1 - y_2)^2 + (\phi_1 - \phi_2)^2}$ is the distance between the subjets in the y-ϕ plane, and $R = 0.4$ is the jet radius. The parameters z_{cut} and β control the grooming procedure. If the Soft Drop condition is satisfied, the corresponding pair of subjets is retained as the final groomed jet. Otherwise, the subjet with a higher p_{T} is further declustered, and the procedure is repeated until the condition is satisfied. The final groomed subjets were used to measure the jet substructure properties.

In this study, groomed jet observables, including the jet splitting momentum fraction z_{g} [43] and the ratio of the groomed jet mass to the ungroomed jet transverse momentum $M_{\mathrm{g}}/p_{\mathrm{T,jet}}$ [48], were calculated using the AMPT model with a jet-triggering technique. The jet splitting momentum fraction z_{g} is defined as

$$z_{\mathrm{g}} = \frac{\min(p_{\mathrm{T},1}, p_{\mathrm{T},2})}{p_{\mathrm{T},1} + p_{\mathrm{T},2}}, \tag{4}$$

where $p_{\mathrm{T},1}$ and $p_{\mathrm{T},2}$ are the transverse momenta of the two subjets. This definition is identical to that on the left side of Eq. (3) when the subjets satisfy the Soft Drop condition. The groomed jet mass M_{g} is defined as

$$M_{\mathrm{g}} = \sqrt{(E_1 + E_2)^2 - (\vec{p}_1 + \vec{p}_2)^2}, \tag{5}$$

where E_i and $\vec{p}_i$ are the energy and three-momentum vectors of the subjets, respectively. To reconstruct the jet substructure, two sets of Soft Drop grooming parameters are employed, each probing distinct regions of the subjet phase space in the Lund plane [95, 96]. The first setup, with ($z_{\mathrm{cut}} = 0.1$ and $\beta = 0.0$), imposes a grooming condition based solely on the energy fraction between subjets to capture both the jet core and peripheral modification. It is utilized for analyzing both z_{g} and $M_{\mathrm{g}}/p_{\mathrm{T,jet}}$ observables. The second setup, which employs a stronger grooming condition ($z_{\mathrm{cut}} = 0.5$, $\beta = 1.5$), reduces the contribution from large-angle subjets, thereby enhancing the sensitivity to the jet core region. This configuration is employed exclusively in the $M_{\mathrm{g}}/p_{\mathrm{T,jet}}$ analysis. An additional angular requirement of $\Delta R_{12} > 0.1$ is imposed across all measurements to suppress unphysical contributions, following the CMS experimental procedure [43, 48]. Furthermore, the z_{g} and $M_{\mathrm{g}}/p_{\mathrm{T,jet}}$ distributions were normalized by the number of groomed jets ($N_{\mathrm{g,jet}}$). We have verified that treating jet constituents as either massive or massless results in very similar z_{g} and $M_{\mathrm{g}}/p_{\mathrm{T,jet}}$ distributions. To facilitate a more direct comparison between the two grooming configurations, Fig. 1 presents the joint distributions of z_{g} and ΔR_{12} for jets that satisfy the Soft Drop condition defined in Eq. (3). The distributions include an angular cut of $\Delta R_{12} > 0.1$ and are normalized by $\frac{1}{N_{\mathrm{g,jet}}} \frac{\mathrm{d}^2 N_{\mathrm{g,jet}}}{\mathrm{d}\ln(1/\Delta R_{12})\,\mathrm{d}\ln(1/z_{\mathrm{g}})}$. The comparison is performed within the jet transverse momentum range of $140 < p_{\mathrm{T,jet}} < 160$ GeV in pp collisions at $\sqrt{s} = 5.02$ TeV using the AMPT model. Relative to the first setup ($z_{\mathrm{cut}} = 0.1$, $\beta = 0.0$), the stronger grooming configuration ($z_{\mathrm{cut}} = 0.5$, $\beta = 1.5$) exhibits a clearly depleted region in the upper-left part of the distribution, corresponding to a reduction in subjets with

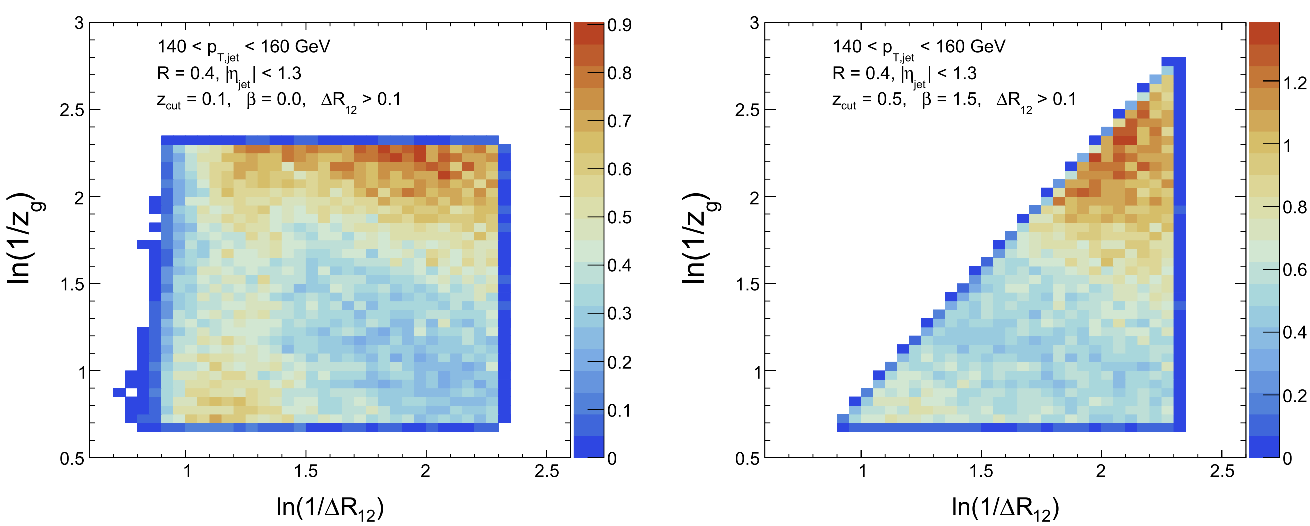

Fig. 1 (Color online) Comparison of two Soft Drop grooming parameter settings: $z_{\mathrm{cut}} = 0.1$ and $\beta = 0.0$ (left panel) and $z_{\mathrm{cut}} = 0.5$ and $\beta = 1.5$ (right panel), with an angular cut of $\Delta R_{12} > 0.1$, for jets in the transverse momentum range $140 < p_{\mathrm{T,jet}} < 160$ GeV in pp collisions at $\sqrt{s} = 5.02$ TeV

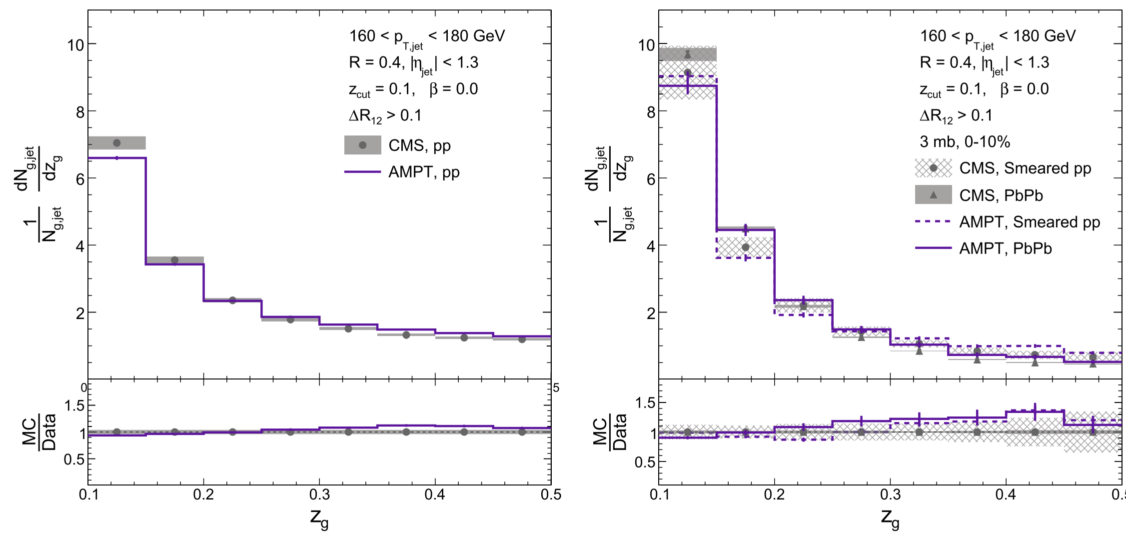

Fig. 2 Distributions of the z_g in pp collisions (left panel) and in 0–10% smeared pp and PbPb collisions (right panel), within the jet transverse momentum range of $160 < p_{T,jet} < 180$ GeV at $\sqrt{s_{NN}} = 5.02$ TeV. The Soft Drop grooming parameters are set to $z_{cut} = 0.1$ and $\beta = 0.0$, with an angular cut of $\Delta R_{12} > 0.1$. Lines represent the AMPT model results, while data points correspond to CMS measurements [43], with statistical uncertainties shown as error bars and systematic uncertainties as shaded bands

large angular separation. This indicates an increased focus on the jet core region.

3 Results and discussion

3.1 Jet splitting momentum fraction

We compare the z_g distributions obtained using the first set of Soft Drop grooming parameters ($z_{cut} = 0.1$, $\beta = 0.0$) from the AMPT model with CMS measurements [43] at $\sqrt{s_{NN}} = 5.02$ TeV, as shown in Fig. 2. The left panel shows the comparison for pp collisions in the jet transverse momentum range of $160 < p_{T,jet} < 180$ GeV. The AMPT results are in good agreement with the CMS data, providing a reliable baseline. The right panel presents the z_g distributions for 0–10% most central smeared pp and PbPb collisions in the same $p_{T,jet}$ range. Here, AMPT simulations were performed with partonic interactions of 3 mb. The centrality of smeared pp events is determined based on the multiplicity distributions from the PbPb collisions without applying jet triggers. Compared to the CMS data, the AMPT predictions exhibited a slightly flatter z_g distribution.

Figure 3 displays the ratios of z_g distributions between PbPb and smeared pp collisions at $\sqrt{s_{NN}} = 5.02$ TeV, shown for different centrality bins (left panel) and jet transverse momentum ranges (right panel). Two scenarios are considered: simulations with partonic interactions for 3 mb and without partonic interactions for 0 mb. In the left panel, for jets with $160 < p_{T,jet} < 180$ GeV, no modification is observed across all centrality bins when partonic interactions are turned off. In contrast, simulations with partonic interactions exhibit negligible changes in peripheral PbPb collisions, whereas a slight enhancement in asymmetric splitting is observed in more central PbPb collisions. These results are qualitatively consistent with the CMS measurements, within the uncertainties. The right panel illustrates the z_g modification for different $p_{T,jet}$ ranges in the 0–10% most central collisions. For partonic interactions of 0 mb, the z_g distributions remain largely unmodified across the $p_{T,jet}$ range of 140–200 GeV, with only minor deviations observed at higher jet momenta ($200 < p_{T,jet} < 250$ GeV). When partonic interactions are included, slight modifications appear throughout the full $p_{T,jet}$ range, indicating a weak sensitivity of z_g to jet–medium interactions, particularly at low $p_{T,jet}$.

Furthermore, several theoretical studies have explored the behavior of the z_g observable in the high jet transverse momentum regime ($p_{T,jet} > 140$ GeV) in comparison with CMS measurements [43]. Simulations using JEWEL with the four-momentum subtraction method [51], which incorporates medium response effects, predict a mild shift of the z_g distribution toward smaller values. Similarly, calculations based on the SCET incorporating Glauber gluon interactions [52] also revealed a slight enhancement in the probability of asymmetric splittings. At lower jet transverse momentum ($60 < p_{T,jet} < 100$ GeV), the ALICE experiment [45] observed no significant modification of the z_g distribution in PbPb collisions relative to pp collisions when using strong grooming settings ($z_{cut} = 0.2$, $\beta = 0.0$). These results are consistent with predictions from JETSCAPE [53], which combines the MATTER model [97] for high-virtuality

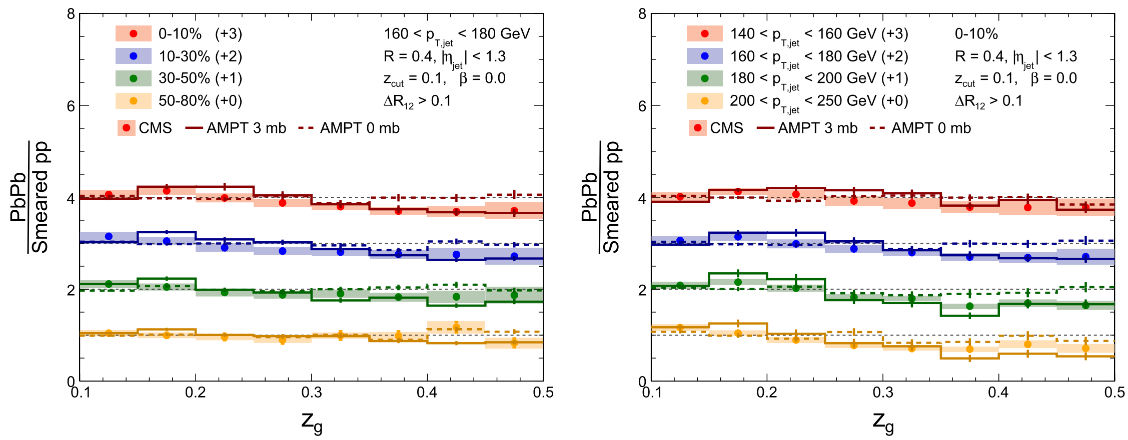

Fig. 3 (Color online) Ratios of the z_g distributions between PbPb and smeared pp collisions at $\sqrt{s_{NN}} = 5.02$ TeV, for different centrality bins (left panel) and jet transverse momentum ranges (right panel). The Soft Drop grooming parameters are set to $z_{cut} = 0.1$ and $\beta = 0.0$, with an angular cut of $\Delta R_{12} > 0.1$. Solid (3 mb) and dashed (0 mb) lines represent the AMPT model results, while data points correspond to CMS measurements [43], with statistical uncertainties shown as error bars and systematic uncertainties as shaded bands

parton evolution and the LBT model [42, 98] for low virtuality in jet–medium interactions. Interestingly, the higher twist formalism [54], which is based on the coherent energy loss assumption for the two split subjets, predicts a non-monotonic dependence of the z_g modification on the jet energy: The strongest modification occurs at intermediate jet energies, while both lower and higher energies exhibit weaker effects.

3.2 Groomed jet mass

We further investigate the ratio of the groomed jet mass to ungroomed jet transverse momentum, $M_g/p_{T,jet}$, using two sets of Soft Drop grooming parameters at $\sqrt{s_{NN}} = 5.02$ TeV, and compare our results with the CMS data [48]. Figure 4 presents the $M_g/p_{T,jet}$ distributions in pp collisions (top panels) and in both smeared pp and PbPb collisions with partonic interactions of 3 mb (bottom panels), for jets in $p_{T,jet}$ range of 160–180 GeV. In the top panels, our simulations agree well with the CMS results within uncertainties, providing a reliable baseline for further comparison. Additionally, the $M_g/p_{T,jet}$ distributions with the Soft Drop parameters $z_{cut} = 0.5$ and $\beta = 1.5$ (top right panel) appear steeper than those with $z_{cut} = 0.1$ and $\beta = 0.0$ (top left panel), reflecting a stronger grooming constraint focused on the jet core. In the bottom left panel, corresponding to the first grooming condition, we observe a broadening of the $M_g/p_{T,jet}$ distribution in PbPb collisions compared to smeared pp collisions. The smeared pp result exhibits a minor deviation, while the PbPb result presents an enhancement at high $M_g/p_{T,jet}$ in comparison with CMS data. For the second grooming condition, shown in the bottom right panel, the smeared pp result remains consistent with the CMS data within uncertainties, while the PbPb events display a deviation in the $M_g/p_{T,jet}$ distribution compared to the CMS measurement.

Figure 5 shows the ratios of $M_g/p_{T,jet}$ distributions between PbPb and smeared pp collisions in the jet transverse momentum range of $160 < p_{T,jet} < 180$ GeV at $\sqrt{s_{NN}} = 5.02$ TeV, for different centrality bins, using two Soft Drop grooming parameters: a condition sensitive only to the energy fraction between subjets ($z_{cut} = 0.1$, $\beta = 0.0$) in the left panel and a stronger grooming setup that emphasizes the jet core structure ($z_{cut} = 0.5$, $\beta = 1.5$) in the right panel. Simulations were performed both with (3 mb) and without (0 mb) partonic interactions, consistent with the approach taken in the z_g analysis. In the left panel, when partonic interactions are turned off, the ratio remains flat across all centrality classes, except for fluctuations in the highest $M_g/p_{T,jet}$ bin. However, when partonic interactions are included, a hint of enhancement emerges in the high $M_g/p_{T,jet}$ region, particularly in more central collisions, indicating medium-induced broadening of the groomed jet mass. In contrast, the stronger grooming condition shown in the right panel leads to no significant modification in any centrality bin, regardless of the presence of partonic interactions. This confirms that the observed enhancement is predominantly associated with the medium response located at larger angles from the jet axis.

To further investigate the sensitivity to the jet transverse momentum, Fig. 6 displays the modification ratio of $M_g/p_{T,jet}$ distribution for the 0–10% most central PbPb collisions relative to smeared pp collisions for different $p_{T,jet}$. For the first grooming condition (left panel), simulations without partonic interactions again show no modification, except for minor fluctuations in the highest $M_g/p_{T,jet}$ bin at

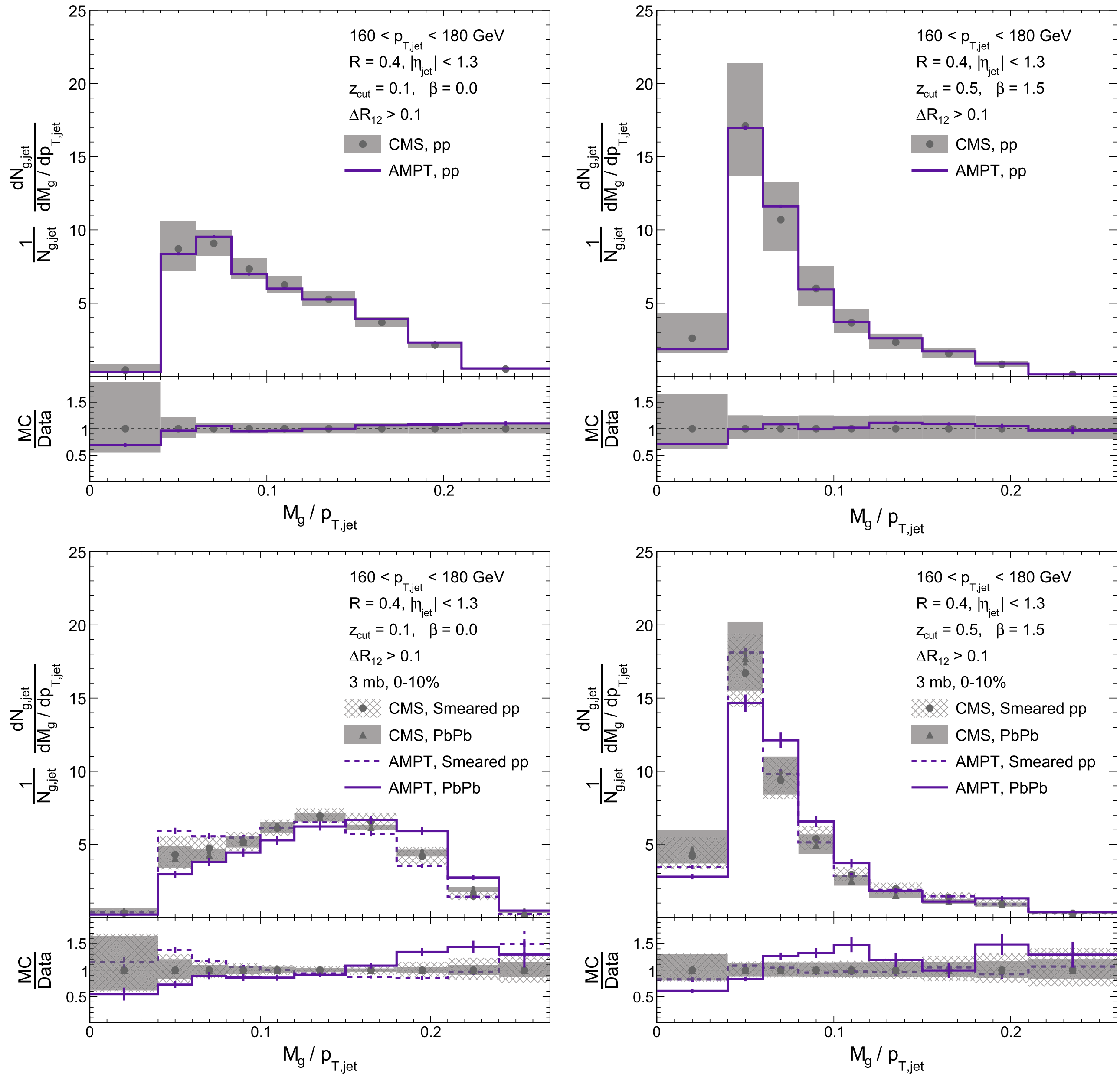

Fig. 4 Distributions of the $M_g/p_{T,jet}$ in pp collisions (top panels) and in 0–10% smeared pp and PbPb collisions (bottom panels) within the jet transverse momentum range of $160 < p_{T,jet} < 180$ GeV at $\sqrt{s_{NN}} = 5.02$ TeV. The Soft Drop grooming parameters are set to $z_{cut} = 0.1$, $\beta = 0.0$ (left panels) and $z_{cut} = 0.5$, $\beta = 1.5$ (right panels), with an angular cut of $\Delta R_{12} > 0.1$. Lines represent the AMPT model results, while data points correspond to CMS measurements [48], with statistical uncertainties shown as error bars and systematic uncertainties as shaded bands

intermediate $p_{T,jet}$. In contrast, when partonic interactions are included, a noticeable enhancement is observed in the low $p_{T,jet}$ region, consistent with CMS measurements. This suggests that the elastic interactions between the jets and medium partons contribute to an increase in the groomed jet mass. No significant changes are observed across all $p_{T,jet}$ intervals under the stronger grooming condition (right panel), further confirming that medium-induced modifications are primarily attributed to the large-angle scattering within the AMPT framework.

To elucidate the origin of these modifications, we further analyzed the evolution of the ratio of $M_g/p_{T,jet}$ distribution at four dynamic stages in the AMPT model: initial state, after parton cascade, after hadronization, and after hadronic rescatterings, as shown in Fig. 7. The analysis focuses on jets with $160 < p_{T,jet} < 180$ GeV in 0–10% most central PbPb and smeared pp events. For the first grooming condition (top

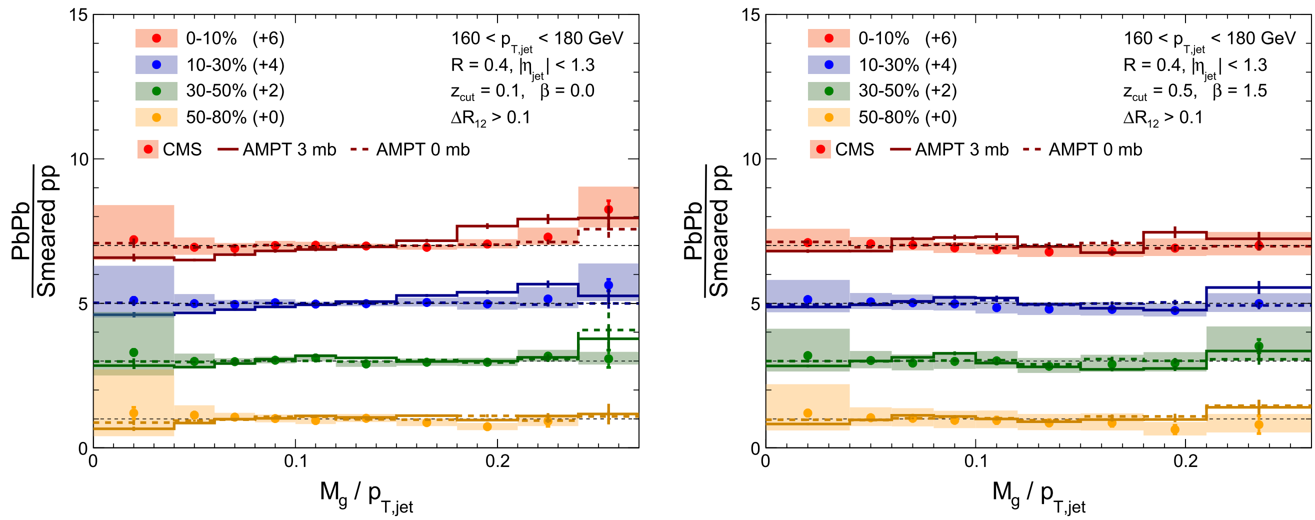

Fig. 5 (Color online) Ratios of the $M_g/p_{T,jet}$ distributions between PbPb and smeared pp collisions in the jet transverse momentum range of $160 < p_{T,jet} < 180$ GeV at $\sqrt{s_{NN}} = 5.02$ TeV, for different centrality bins. The Soft Drop grooming parameters are set to $z_{cut} = 0.1$, $\beta = 0.0$ (left panel) and $z_{cut} = 0.5$, $\beta = 1.5$ (right panel), with an angular cut of $\Delta R_{12} > 0.1$. Solid (3 mb) and dashed (0 mb) lines represent the AMPT model results, while data points correspond to CMS measurements [48], with statistical uncertainties shown as error bars and systematic uncertainties as shaded bands

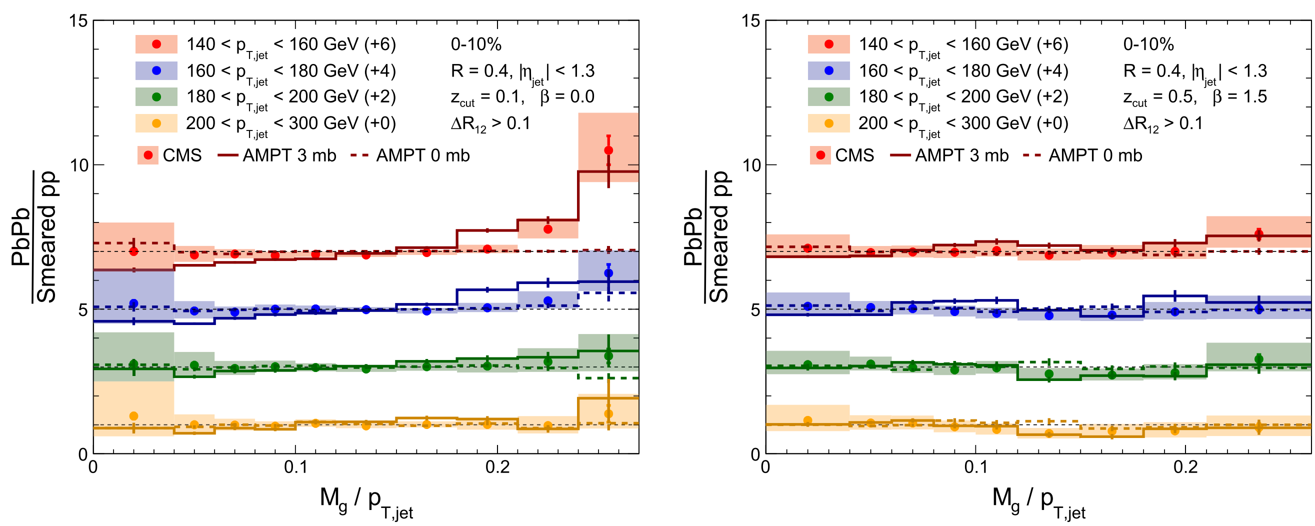

Fig. 6 (Color online) Ratios of the $M_g/p_{T,jet}$ distributions between 0–10% PbPb and smeared pp collisions at $\sqrt{s_{NN}} = 5.02$ TeV, for different jet transverse momentum ranges. The Soft Drop grooming parameters are set to $z_{cut} = 0.1$, $\beta = 0.0$ (left panel) and $z_{cut} = 0.5$, $\beta = 1.5$ (right panel), with an angular cut of $\Delta R_{12} > 0.1$. Solid (3 mb) and dashed (0 mb) lines represent the AMPT model results, while data points correspond to CMS measurements [48], with statistical uncertainties shown as error bars and systematic uncertainties as shaded bands

left panel), no modification is observed in the initial state, while a pronounced enhancement in the ratio of $M_g/p_{T,jet}$ distribution emerges immediately after the parton cascade stage (3 mb), confirming that jet–medium interactions are the primary drivers of the modification. The hadronization and hadronic rescattering stages retain the enhancement, but their additional effects are minor, consistent with the ability of the grooming procedure to suppress non-perturbative contributions. In contrast, for simulations without partonic interactions (bottom left panel), no noticeable change is observed across any stage, reaffirming the absence of jet quenching effects. The results using the second grooming condition are shown in the right panels, where only minor deviations are observed, further emphasizing that the groomed jet mass is sensitive to the medium response located at larger angles from the jet axis.

In summary, our analysis demonstrates that jet–medium interactions lead to a significant enhancement in the groomed jet mass. This effect has been investigated using several theoretical frameworks. JEWEL simulations [55] fail

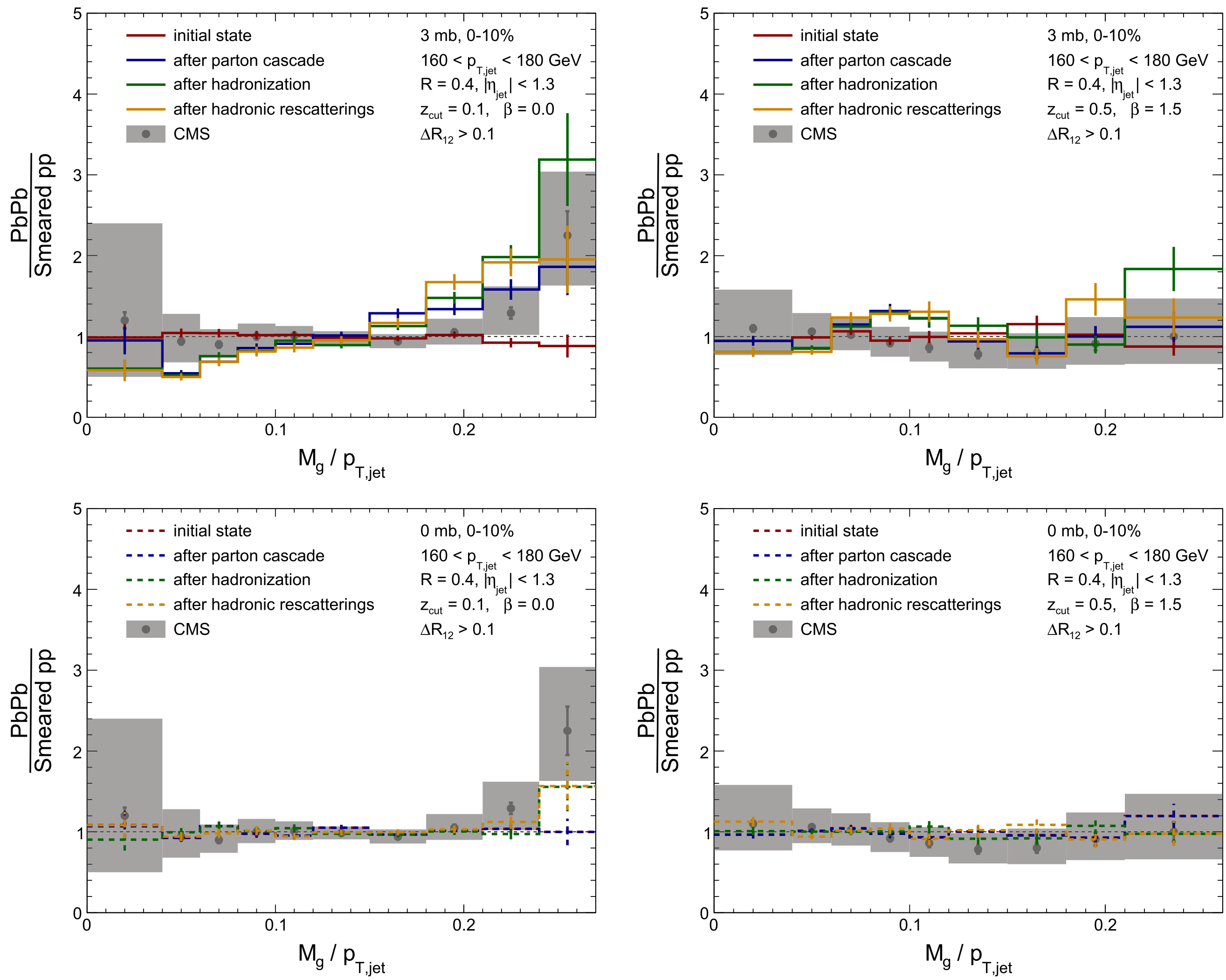

Fig. 7 Ratios of the $M_g/p_{\mathrm{T,jet}}$ distributions between 0–10% PbPb and smeared pp collisions in the jet transverse momentum range of $160 < p_{\mathrm{T,jet}} < 180$ GeV within four dynamical evolution stages at $\sqrt{s_{\mathrm{NN}}} = 5.02$ TeV. The Soft Drop grooming parameters are set to $z_{\mathrm{cut}} = 0.1$, $\beta = 0.0$ (left panels) and $z_{\mathrm{cut}} = 0.5$, $\beta = 1.5$ (right panels), with an angular cut of $\Delta R_{12} > 0.1$. Lines represent the AMPT model results with parton cross section of 3 mb (top panels) and 0 mb (bottom panels), while data points correspond to CMS measurements [48], with statistical uncertainties shown as error bars and systematic uncertainties as shaded bands

to describe the smeared pp and PbPb results, in comparison with CMS data [48]. Nevertheless, the medium response in JEWEL still leads to a noticeable enhancement at large $M_g/p_{\mathrm{T,jet}}$ values [48]. Similarly, the LBT model [56] predicts a substantial enhancement in the tail of the groomed jet mass distribution owing to the medium response. When comparing with ALICE data [50], Hybrid model [57], based on a strongly coupled AdS/CFT framework, shows that the elastic Molière scattering [58] generates large-angle jet constituents and broadens the groomed jet mass distributions. These results collectively highlight the strong sensitivity of the groomed jet mass to jet–medium interactions, making it a powerful observable for probing QGP properties.

4 Summary

In this study, we explored jet substructure observables in pp and PbPb collisions at $\sqrt{s_{\mathrm{NN}}} = 5.02$ TeV using the AMPT model with the string melting mechanism. Background effects in relativistic heavy-ion collisions were mitigated using the constituent subtraction method for both PbPb and smeared pp events. The analysis focused on two groomed jet observables reconstructed via the Soft Drop algorithm: the jet splitting momentum fraction (z_g) and the ratio of the groomed jet mass to the ungroomed jet transverse momentum ($M_g/p_{\mathrm{T,jet}}$). Two sets of grooming parameters were employed to probe the sensitivity of these observables to the jet–medium interactions. The simulation results were compared with the CMS data.

Our simulations reproduce the z_g and $M_g/p_{T,jet}$ distributions in pp collisions, establishing the AMPT model as a reliable baseline for future studies. With the Soft Drop parameters $z_{cut} = 0.1$ and $\beta = 0.0$, a slight enhancement of asymmetric splittings in the z_g distribution is observed in central PbPb collisions relative to smeared pp events, in qualitative agreement with CMS measurements. In contrast, a more significant modification is found in the $M_g/p_{T,jet}$ distribution, particularly in more central events and at lower jet transverse momentum. By tracing the dynamical evolution of the jet substructure through the different stages in the AMPT model, we found that this enhancement originates primarily from the parton cascade stage, where elastic scatterings between the jet and medium partons dominate. The contributions from hadronization and hadronic rescatterings are strongly suppressed by the grooming procedure. Furthermore, simulations with the stronger grooming constraint ($z_{cut} = 0.5$, $\beta = 1.5$) show no significant changes, underscoring that the medium-induced modifications are predominantly associated with large-angle scattering within the AMPT framework. Moreover, previous AMPT studies [84, 85] have emphasized the role of elastic interactions in transporting energy from the hard jet core to larger angles than the jet axis. Incorporating inelastic radiative energy loss processes into the parton cascade is expected to enhance soft gluon radiation and result in more small-angle splittings, as reflected in the jet splitting radius (r_g) [45, 53] during jet–medium interactions. This represents a crucial direction for the future development of the AMPT framework in this area.

Acknowledgements We thank Prof. Bin Wu for helpful discussions and Dr. Chen Zhong for maintaining the high-quality performance of the Fudan supercomputing platform for nuclear physics.

Author Contributions All authors contributed to the study conception and design. Material preparation, data collection, and analysis were performed by Xiang-Pan Duan. The first draft of the manuscript was written by Xiang-Pan Duan, and all authors commented on previous versions of the manuscript. All authors read and approved the final manuscript.

Data Availability The data that support the findings of this study are openly available in Science Data Bank at https://cstr.cn/31253.11.sciencedb.j00186.00952 and https://doi.org/10.57760/sciencedb.j00186.00952.

Declarations

Conflict of interest The authors declare that they have no conflict of interest.

References

1. I. Arsene, I.G. Bearden, D. Beavis et al., Quark gluon plasma and color glass condensate at RHIC? The Perspective from the BRAHMS experiment. Nucl. Phys. A **757**, 1–27 (2005). https://doi.org/10.1016/j.nuclphysa.2005.02.130
2. PHOBOS Collaboration , B.B. Back, M.D. Baker et al., The PHOBOS perspective on discoveries at RHIC. Nucl. Phys. A **757**, 28–101 (2005). https://doi.org/10.1016/j.nuclphysa.2005.03.084
3. PHENIX Collaboration, K. Adcox, S.S. Adler et al., Formation of dense partonic matter in relativistic nucleus-nucleus collisions at RHIC: experimental evaluation by the PHENIX collaboration. Nucl. Phys. A **757**, 184–283 (2005). https://doi.org/10.1016/j.nuclphysa.2005.03.086
4. STAR Collaboration, J. Adams, M.M. Aggarwal et al., Experimental and theoretical challenges in the search for the quark gluon plasma: the STAR Collaboration's critical assessment of the evidence from RHIC collisions. Nucl. Phys. A **757**, 102–183 (2005). https://doi.org/10.1016/j.nuclphysa.2005.03.085
5. K.J. Eskola, H. Paukkunen, C.A. Salgado, An Improved global analysis of nuclear parton distribution functions including RHIC data. J. High Energy Phys. **07**, 102 (2008). https://doi.org/10.1088/1126-6708/2008/07/102
6. X. Luo, N. Xu, Search for the QCD critical point with fluctuations of conserved quantities in relativistic heavy-ion collisions at RHIC: an overview. Nucl. Sci. Tech. **28**, 112 (2017). https://doi.org/10.1007/s41365-017-0257-0
7. C. Shen, L. Yan, Recent development of hydrodynamic modeling in heavy-ion collisions. Nucl. Sci. Tech. **31**, 122 (2020). https://doi.org/10.1007/s41365-020-00829-z
8. J. Chen, X. Dong, X. He et al., Properties of the QCD matter: review of selected results from the relativistic heavy ion collider beam energy scan (RHIC BES) program. Nucl. Sci. Tech. **35**, 214 (2024). https://doi.org/10.1007/s41365-024-01591-2
9. G. Aad, B. Abbott, J. Abdallah et al., Observation of a centrality-dependent dijet asymmetry in lead-lead collisions at $\sqrt{s_{NN}} = 2.77$ TeV with the ATLAS detector at the LHC. Phys. Rev. Lett. **105**, 252303 (2010). https://doi.org/10.1103/PhysRevLett.105.252303
10. ALICE Collaboration, K. Aamodt, A. Abrahantes Quintana et al., Suppression of charged particle production at large transverse momentum in central Pb-Pb collisions at $\sqrt{s_{NN}} = 2.76$ TeV. Phys. Lett. B **696**, 30–39 (2011). https://doi.org/10.1016/j.physletb.2010.12.020
11. The CMS Collaboration, S. Chatrchyan, V. Khachatryan et al., Study of High-pT charged particle suppression in PbPb compared to pp collisions at $\sqrt{s_{NN}} = 2.76$ TeV. Eur. Phys. J. C **72**, 1945 (2012). https://doi.org/10.1140/epjc/s10052-012-1945-x
12. H. Song, Y. Zhou, K. Gajdosova, Collective flow and hydrodynamics in large and small systems at the LHC. Nucl. Sci. Tech. **28**, 99 (2017). https://doi.org/10.1007/s41365-017-0245-4
13. Q.Y. Shou, Y.G. Ma, S. Zhang et al., Properties of QCD matter: a review of selected results from ALICE experiment. Nucl. Sci. Tech. **35**, 219 (2024). https://doi.org/10.1007/s41365-024-01583-2
14. X.P. Duan, L. Chen, G.L. Ma, et al., KNO scaling in quark and gluon jets at the LHC. arXiv:2503.24200
15. M. Gyulassy, L. McLerran, New forms of QCD matter discovered at RHIC. Nucl. Phys. A **750**, 30–63 (2005). https://doi.org/10.1016/j.nuclphysa.2004.10.034
16. W.B. He, Y.G. Ma, L.G. Pang et al., High-energy nuclear physics meets machine learning. Nucl. Sci. Tech. **34**, 88 (2023). https://doi.org/10.1007/s41365-023-01233-z
17. G.F. Sterman, S. Weinberg, Jets from quantum chromodynamics. Phys. Rev. Lett. **39**, 1436 (1977). https://doi.org/10.1103/PhysRevLett.39.1436
18. R.P. Feynman, R.D. Field, G.C. Fox, A quantum chromodynamic approach for the large transverse momentum production of particles and jets. Phys. Rev. D **18**, 3320 (1978). https://doi.org/10.1103/PhysRevD.18.3320

19. M. Gyulassy, M. Plumer, Jet quenching in dense matter. Phys. Lett. B **243**, 432–438 (1990). https://doi.org/10.1016/0370-2693(90)91409-5
20. X.N. Wang, M. Gyulassy, Gluon shadowing and jet quenching in $A + A$ collisions at $\sqrt{s} = = 200A$-GeV. Phys. Rev. Lett. **68**, 1480–1483 (1992). https://doi.org/10.1103/PhysRevLett.68.1480
21. R. Baier, Y.L. Dokshitzer, A.H. Mueller et al., Radiative energy loss and p⊥ broadening of high-energy partons in nuclei. Nucl. Phys. B **484**, 265–282 (1997). https://doi.org/10.1016/S0550-3213(96)00581-0
22. C.A. Salgado, U.A. Wiedemann, A dynamical scaling law for jet tomography. Phys. Rev. Lett. **89**, 092303 (2002). https://doi.org/10.1103/PhysRevLett.89.092303
23. C.A. Salgado, U.A. Wiedemann, Calculating quenching weights. Phys. Rev. D **68**, 014008 (2003). https://doi.org/10.1103/PhysRevD.68.014008
24. N. Armesto, A. Dainese, C.A. Salgado et al., Testing the color charge and mass dependence of parton energy loss with heavy-to-light ratios at RHIC and CERN LHC. Phys. Rev. D **71**, 054027 (2005). https://doi.org/10.1103/PhysRevD.71.054027
25. J. Casalderrey-Solana, C.A. Salgado, Introductory lectures on jet quenching in heavy ion collisions. Acta Phys. Polon. B **38**, 3731–3794 (2007)
26. G.Y. Qin, X.N. Wang, Jet quenching in high-energy heavy-ion collisions. Int. J. Mod. Phys. E **24**, 1530014 (2015). https://doi.org/10.1142/S0218301315300143
27. S. Cao, X.N. Wang, Jet quenching and medium response in high-energy heavy-ion collisions: a review. Rept. Prog. Phys. **84**, 024301 (2021). https://doi.org/10.1088/1361-6633/abc22b
28. J. Adams, C. Adler, M.M. Aggarwal et al., Transverse momentum and collision energy dependence of high p(T) hadron suppression in Au+Au collisions at ultrarelativistic energies. Phys. Rev. Lett. **91**, 172302 (2003). https://doi.org/10.1103/PhysRevLett.91.172302
29. K.J. Eskola, H. Honkanen, C.A. Salgado et al., The Fragility of high-p(T) hadron spectra as a hard probe. Nucl. Phys. A **747**, 511–529 (2005). https://doi.org/10.1016/j.nuclphysa.2004.09.070
30. S. Cao, T. Luo, G.Y. Qin et al., Heavy and light flavor jet quenching at RHIC and LHC energies. Phys. Lett. B **777**, 255–259 (2018). https://doi.org/10.1016/j.physletb.2017.12.023
31. M. Aaboud et al., Measurement of the nuclear modification factor for inclusive jets in Pb+Pb collisions at $\sqrt{s_{\rm NN}} = 5.02$ TeV with the ATLAS detector. Phys. Lett. B **790**, 108–128 (2019). https://doi.org/10.1016/j.physletb.2018.10.076
32. Y. He, S. Cao, W. Chen et al., Interplaying mechanisms behind single inclusive jet suppression in heavy-ion collisions. Phys. Rev. C **99**, 054911 (2019). https://doi.org/10.1103/PhysRevC.99.054911
33. W. Zhao, W. Ke, W. Chen et al., From hydrodynamics to jet quenching, coalescence, and hadron cascade: a coupled approach to solving the RAA⊗v2 puzzle. Phys. Rev. Lett. **128**, 022302 (2022). https://doi.org/10.1103/PhysRevLett.128.022302
34. S.P. Adhya, C.A. Salgado, M. Spousta et al., Multi-partonic medium induced cascades in expanding media. Eur. Phys. J. C **82**, 20 (2022). https://doi.org/10.1140/epjc/s10052-021-09950-8
35. S.L. Zhang, H. Xing, J/ψ production within a jet in high-energy proton-proton and nucleus-nucleus collisions. Phys. Lett. B **863**, 139382 (2025). https://doi.org/10.1016/j.physletb.2025.139382
36. G.Y. Qin, B. Muller, Explanation of Di jet asymmetry in Pb+Pb collisions at the Large Hadron Collider. Phys. Rev. Lett. **106**, 162302 (2011). https://doi.org/10.1103/PhysRevLett.106.162302. (**Erratum: Phys. Rev. Lett. 108, 189904 (2012).**)
37. G.L. Ma, Dijet asymmetry in Pb+Pb collisions at $\sqrt{s_{NN}}$=2.76 TeV within a multiphase transport model. Phys. Rev. C **87**, 064901 (2013). https://doi.org/10.1103/PhysRevC.87.064901
38. L. Chen, G.Y. Qin, S.Y. Wei et al., Dijet asymmetry in the resummation improved perturbative QCD approach. Phys. Lett. B **782**, 773–778 (2018). https://doi.org/10.1016/j.physletb.2018.06.002
39. L. Chen, G.Y. Qin, L. Wang et al., Study of isolated-photon and jet momentum imbalance in *pp* and *PbPb* collisions. Nucl. Phys. B **933**, 306–319 (2018). https://doi.org/10.1016/j.nuclphysb.2018.06.013
40. L. Chen, S.Y. Wei, H.Z. Zhang, Probing jet medium interactions via $Z(H)$ + jet momentum imbalances. Eur. Phys. J. C **80**, 1136 (2020). https://doi.org/10.1140/epjc/s10052-020-08702-4
41. Z.Q. Liu, H. Zhang, B.W. Zhang et al., Quantifying jet transport properties via large $p_{\rm T}$ hadron production. Eur. Phys. J. C **76**, 20 (2016). https://doi.org/10.1140/epjc/s10052-016-3885-3
42. T. Luo, Y. He, S. Cao et al., Linear Boltzmann transport for jet propagation in the quark-gluon plasma: inelastic processes and jet modification. Phys. Rev. C **109**, 034919 (2024). https://doi.org/10.1103/PhysRevC.109.034919
43. A.M. Sirunyan, A. Tumasyan, W. Adam et al., Measurement of the splitting function in *pp* and Pb-Pb collisions at $\sqrt{s_{_{\rm NN}}} = 5.02$ TeV. Phys. Rev. Lett. **120**, 142302 (2018). https://doi.org/10.1103/PhysRevLett.120.142302
44. J. Adam, L. Adamczyk, J.R. Adams et al., Measurement of groomed jet substructure observables in p+p collisions at $\sqrt{s}$ =200 GeV with STAR. Phys. Lett. B **811**, 135846 (2020). https://doi.org/10.1016/j.physletb.2020.135846
45. S. Acharya, D. Adamová, A. Adler et al., Measurement of the groomed jet radius and momentum splitting fraction in pp and Pb−Pb collisions at $\sqrt{s_{NN}} = 5.02$ TeV. Phys. Rev. Lett. **128**, 102001 (2022). https://doi.org/10.1103/PhysRevLett.128.102001
46. L. Wang, J.W. Kang, Q. Zhang et al., Jet radius and momentum splitting fraction with dynamical grooming in heavy-ion collisions. Chin. Phys. Lett. **40**, 032101 (2023). https://doi.org/10.1088/0256-307X/40/3/032101
47. B. Blok, C. Wu, z_g distribution for heavy flavor jets in dense quark-gluon plasma. Phys. Rev. D **111**, 074009 (2025). https://doi.org/10.1103/PhysRevD.111.074009
48. The CMS collaboration, A.M. Sirunyan, A. Tumasyan et al., Measurement of the groomed jet mass in PbPb and pp collisions at $\sqrt{s_{\rm NN}} = 5.02$ TeV. JHEP **10**, 161 (2018). https://doi.org/10.1007/JHEP10(2018)161
49. M.S. Abdallah, J. Adam, L. Adamczyk et al., Invariant jet mass measurements in *pp* collisions at $\sqrt{s} = 200$ GeV at RHIC. Phys. Rev. D **104**, 052007 (2021). https://doi.org/10.1103/PhysRevD.104.052007
50. ALICE Collaboration, Medium-induced modification of groomed and ungroomed jet mass and angularities in Pb-Pb collisions at $\sqrt{\rm sNN}$=5.02 TeV. Phys. Lett. B **864**, 139409 (2025). https://doi.org/10.1016/j.physletb.2025.139409
51. G. Milhano, U.A. Wiedemann, K.C. Zapp, Sensitivity of jet substructure to jet-induced medium response. Phys. Lett. B **779**, 409–413 (2018). https://doi.org/10.1016/j.physletb.2018.01.029
52. Y.T. Chien, I. Vitev, Probing the hardest branching within jets in heavy-ion collisions. Phys. Rev. Lett. **119**, 112301 (2017). https://doi.org/10.1103/PhysRevLett.119.112301
53. Y. Tachibana, A. Kumar, A. Majumder et al., Hard jet substructure in a multistage approach. Phys. Rev. C **110**, 044907 (2024). https://doi.org/10.1103/PhysRevC.110.044907
54. N.B. Chang, S. Cao, G.Y. Qin, Probing medium-induced jet splitting and energy loss in heavy-ion collisions. Phys. Lett. B **781**, 423–432 (2018). https://doi.org/10.1016/j.physletb.2018.04.019
55. J.G. Milhano, K. Zapp, Improved background subtraction and a fresh look at jet sub-structure in JEWEL. Eur. Phys. J. C **82**, 1010 (2022). https://doi.org/10.1140/epjc/s10052-022-10954-1

56. T. Luo, Medium response in jet quenching. Nucl. Phys. A **1005**, 121992 (2021). https://doi.org/10.1016/j.nuclphysa.2020.121992
57. J. Casalderrey-Solana, D.C. Gulhan, J.G. Milhano et al., A hybrid strong/weak coupling approach to jet quenching. J. High Energy Phys **10**, 019 (2014). https://doi.org/10.1007/JHEP09(2015)175. (**[Erratum: JHEP 09, 175 (2015)]**)
58. F. D'Eramo, K. Rajagopal, Y. Yin, Molière scattering in quark-gluon plasma: finding point-like scatterers in a liquid. J. High Energy Phys **01**, 172 (2019). https://doi.org/10.1007/JHEP01(2019)172
59. X.P. Duan, G.L. Ma, Search for jet quenching effects on the plain jet mass in Pb+Pb collisions at the LHC with a multiphase transport model. Eur. Phys. J. A **59**, 61 (2023). https://doi.org/10.1140/epja/s10050-023-00970-4
60. Z.W. Lin, C.M. Ko, B.A. Li et al., A multi-phase transport model for relativistic heavy ion collisions. Phys. Rev. C **72**, 064901 (2005). https://doi.org/10.1103/PhysRevC.72.064901
61. Z.W. Lin, L. Zheng, Further developments of a multi-phase transport model for relativistic nuclear collisions. Nucl. Sci. Tech. **32**, 113 (2021). https://doi.org/10.1007/s41365-021-00944-5
62. X.N. Wang, M. Gyulassy, HIJING: a Monte Carlo model for multiple jet production in pp, pA and AA collisions. Phys. Rev. D **44**, 3501–3516 (1991). https://doi.org/10.1103/PhysRevD.44.3501
63. M. Gyulassy, X.N. Wang, HIJING 1.0: a Monte Carlo program for parton and particle production in high-energy hadronic and nuclear collisions. Comput. Phys. Commun. **83**, 307 (1994). https://doi.org/10.1016/0010-4655(94)90057-4
64. T. Sjostrand, High-energy physics event generation with PYTHIA 5.7 and JETSET 7.4. Comput. Phys. Commun. **82**, 74–90 (1994). https://doi.org/10.1016/0010-4655(94)90132-5
65. B. Andersson, G. Gustafson, B. Soderberg, A general model for jet fragmentation. Z. Phys. C **20**, 317 (1983). https://doi.org/10.1007/BF01407824
66. B. Andersson, G. Gustafson, G. Ingelman et al., Parton fragmentation and string dynamics. Phys. Rept. **97**, 31–145 (1983). https://doi.org/10.1016/0370-1573(83)90080-7
67. D.W. Duke, J.F. Owens, Q^2 dependent parametrizations of parton distribution functions. Phys. Rev. D **30**, 49–54 (1984). https://doi.org/10.1103/PhysRevD.30.49
68. J.F. Owens, Large momentum transfer production of direct photons, jets, and particles. Rev. Mod. Phys. **59**, 465 (1987). https://doi.org/10.1103/RevModPhys.59.465
69. B. Zhang, ZPC 1.0.1: a Parton cascade for ultrarelativistic heavy ion collisions. Comput. Phys. Commun. **109**, 193–206 (1998). https://doi.org/10.1016/S0010-4655(98)00010-1
70. B.A. Li, C.M. Ko, Formation of superdense hadronic matter in high-energy heavy ion collisions. Phys. Rev. C **52**, 2037–2063 (1995). https://doi.org/10.1103/PhysRevC.52.2037
71. G.L. Ma, A. Bzdak, Long-range azimuthal correlations in proton–proton and proton–nucleus collisions from the incoherent scattering of partons. Phys. Lett. B **739**, 209–213 (2014). https://doi.org/10.1016/j.physletb.2014.10.066
72. A. Bzdak, G.L. Ma, Elliptic and triangular flow in p+Pb and peripheral Pb+Pb collisions from parton scatterings. Phys. Rev. Lett. **113**, 252301 (2014). https://doi.org/10.1103/PhysRevLett.113.252301
73. P. Bozek, A. Bzdak, G.L. Ma, Rapidity dependence of elliptic and triangular flow in proton–nucleus collisions from collective dynamics. Phys. Lett. B **748**, 301–305 (2015). https://doi.org/10.1016/j.physletb.2015.06.007
74. L. He, T. Edmonds, Z.W. Lin et al., Anisotropic parton escape is the dominant source of azimuthal anisotropy in transport models. Phys. Lett. B **753**, 506–510 (2016). https://doi.org/10.1016/j.physletb.2015.12.051
75. X.P. Duan, W.Y. Wu, Y. Zhou et al., Unraveling the partonic flow in small systems with an improved multi-phase transport model. PoS **2024**, 634 (2025). https://doi.org/10.22323/1.476.0634
76. G.L. Ma, Towards detailed tomography of high energy heavy-ion collisions by γ-jet. Phys. Lett. B **724**, 278–282 (2013). https://doi.org/10.1016/j.physletb.2013.06.029
77. G.L. Ma, Decomposition of the jet fragmentation function in high-energy heavy-ion collisions. Phys. Rev. C **88**, 021902 (2013). https://doi.org/10.1103/PhysRevC.88.021902
78. G.L. Ma, Medium modifications of the photon-tagged jet fragmentation function in high-energy heavy-ion collisions. Phys. Rev. C **89**, 064909 (2014). https://doi.org/10.1103/PhysRevC.89.064909
79. X.P. Duan, W. Zhao, G.L. Ma, Hadronization effects on transverse momentum dependent jet fragmentation function in small systems. Eur. Phys. J. Plus **138**, 669 (2023). https://doi.org/10.1140/epjp/s13360-023-04303-8
80. Y.H. Feng, C.M. Ko, Y.G. Ma et al., Jet-induced enhancement of deuteron production in pp and p-Pb collisions at the LHC. Phys. Lett. B **859**, 139102 (2024). https://doi.org/10.1016/j.physletb.2024.139102
81. G.L. Ma, Medium modifications of jet shapes in Pb+Pb collisions at $\sqrt{s_{_{NN}}}$ = 2.76 TeV within a multiphase transport model. Phys. Rev. C **89**, 024902 (2014). https://doi.org/10.1103/PhysRevC.89.024902
82. M.W. Nie, G.L. Ma, Azimuthal anisotropies of reconstructed jets in Pb+Pb collisions at $\sqrt{s_{_{NN}}}$ = 2.76 TeV in a multiphase transport model. Phys. Rev. C **90**, 014907 (2014). https://doi.org/10.1103/PhysRevC.90.014907
83. F.C. Zhou, G.L. Ma, Y.G. Ma, Extracting jet transport parameter $\hat{q}$ from a multiphase transport model. Eur. Phys. J. A **56**, 70 (2020). https://doi.org/10.1140/epja/s10050-020-00043-w
84. Z. Gao, A. Luo, G.L. Ma et al., Overall momentum balance and redistribution of the lost energy in asymmetric dijet events in 2.76A TeV Pb-Pb collisions with a multiphase transport model. Phys. Rev. C **97**, 044903 (2018). https://doi.org/10.1103/PhysRevC.97.044903
85. A. Luo, Y.X. Mao, G.Y. Qin et al., Jet shape and redistribution of the lost energy from jets in Pb + Pb collisions at the LHC in a multiphase transport model. Eur. Phys. J. C **82**, 156 (2022). https://doi.org/10.1140/epjc/s10052-022-10110-9
86. A. Luo, Y.X. Mao, G.Y. Qin et al., Enhancement of baryon-to-meson ratios around jets as a signature of medium response. Phys. Lett. B **837**, 137638 (2023). https://doi.org/10.1016/j.physletb.2022.137638
87. A. Luo, S. Cao, G.Y. Qin, Probing medium response via strangeness enhancement around quenched jets. Phys. Lett. B **866**, 139520 (2025). https://doi.org/10.1016/j.physletb.2025.139520
88. M. Cacciari, G.P. Salam, G. Soyez, The anti-k_t jet clustering algorithm. JHEP **04**, 063 (2008). https://doi.org/10.1088/1126-6708/2008/04/063
89. M. Cacciari, G.P. Salam, G. Soyez, FastJet user manual. Eur. Phys. J. C **72**, 1896 (2012). https://doi.org/10.1140/epjc/s10052-012-1896-2
90. P. Berta, M. Spousta, D.W. Miller et al., Particle-level pileup subtraction for jets and jet shapes. JHEP **06**, 092 (2014). https://doi.org/10.1007/JHEP06(2014)092
91. G. Soyez, G.P. Salam, J. Kim et al., Pileup subtraction for jet shapes. Phys. Rev. Lett. **110**, 162001 (2013). https://doi.org/10.1103/PhysRevLett.110.162001
92. M. Cacciari, G.P. Salam, Dispelling the N^3 myth for the k_t jet-finder. Phys. Lett. B **641**, 57–61 (2006). https://doi.org/10.1016/j.physletb.2006.08.037
93. A.J. Larkoski, S. Marzani, G. Soyez et al., Soft drop. JHEP **05**, 146 (2014). https://doi.org/10.1007/JHEP05(2014)146

94. Y.L. Dokshitzer, G.D. Leder, S. Moretti et al., Better jet clustering algorithms. JHEP **08**, 001 (1997). https://doi.org/10.1088/1126-6708/1997/08/001
95. F.A. Dreyer, G.P. Salam, G. Soyez, The lund jet plane. JHEP **12**, 064 (2018). https://doi.org/10.1007/JHEP12(2018)064
96. H.A. Andrews et al., Novel tools and observables for jet physics in heavy-ion collisions. J. Phys. G **47**, 065102 (2020). https://doi.org/10.1088/1361-6471/ab7cbc
97. A. Majumder, Incorporating space-time within medium-modified jet event generators. Phys. Rev. C **88**, 014909 (2013). https://doi.org/10.1103/PhysRevC.88.014909
98. Y. He, T. Luo, X.N. Wang et al., Linear Boltzmann transport for jet propagation in the quark-gluon plasma: Elastic processes and medium recoil. Phys. Rev. C **91**, 054908 (2015). https://doi.org/10.1103/PhysRevC.91.054908. (**[Erratum: Phys. Rev. C 97, 019902 (2018)]**)